Applied Catalysis B: Environmental 180 (2016) 471–479

Contents lists available at ScienceDirect

Applied Catalysis B: Environmental

journal homepage: www.elsevier.com/locate/apcatb

Highly active layered double hydroxide-derived cobalt nano-catalysts for *p*-nitrophenol reduction

Hanyu Ma[a,1], Haitao Wang[a,1], Tong Wu[a], Chongzheng Na[a,b,*]

[a] Department of Civil and Environmental Engineering and Earth Sciences, University of Notre Dame, Notre Dame, IN 46556, USA
[b] Department of Civil, Environmental, and Construction Engineering, Texas Tech University, Lubbock, TX 79409, USA

ARTICLE INFO

Article history:
Received 30 March 2015
Received in revised form 25 June 2015
Accepted 26 June 2015
Available online 2 July 2015

Keywords:
Industrial water treatment
Nitroaromatic reduction
Nano catalyst
Non-precious metal catalyst

ABSTRACT

Replacing precious noble-metal catalysts with non-precious metal ones is a well-recognized strategy for reducing the cost of catalytic water treatment. The implementation of this strategy is, however, challenging. To reduce the cost by using non-precious metal catalysts, the reactivity ratio between non-precious and precious metal catalysts must exceed their price ratio. Here, we report for the first time that the parity condition has been surpassed for cobalt (Co), in comparison to the most active precious metal catalyst made of palladium, in the catalytic reduction of *p*-nitrophenol with borohydride. This is achieved by affixing Co nanoparticles on two-dimensional layered double oxide (LDO) nano disks through thermal phase transformation of cobalt-magnesium–aluminum layered double hydroxide precursors. We show that the catalytic activity of LDO–Co is a function of Co molar fraction among metal cations. The highest reactivity is achieved at a molar fraction of 28%, giving a pseudo first order rate constant of 86(±3) min^{-1} at 25 °C for a catalyst dose of 1 g L^{-1} (as Co) and an initial *p*-nitrophenol concentration of 0.2 mM. Compared to other Co nano-catalysts described in the literature, the LDO–Co design has improved the reactivity of cobalt by at least 49 times. We further show that the high reactivity of LDO–Co remains after repeated reuse as well as after borohydride is replaced by formate, a moderate reductant and hydrogen donor. We propose that the high reactivity and superior longevity of LDO–Co are results of the heteroepitaxial fixation of cobalt on LDO through cobalt–oxygen bonds that are similar to those in spinel cobalt oxide.

1. Introduction

An important challenge for developing catalysts for water treatment and environmental remediation is to reduce the cost associated with catalyst fabrication and restocking. One potential solution is replacing the commonly used but expensive 4*d* and 5*d* precious noble metal catalysts such as palladium (Pd) and platinum (Pt) with inexpensive 3*d* non-precious metal catalysts such as cobalt (Co) and nickel (Ni). Because non-precious metal catalysts are usually much less reactive than those made of precious metals, a financial gain can only be made when the ratio of their reactivities exceeds the ratio of their prices. Reaching this cost parity is, however, challenging in spite of recent advances in the design and synthesis of nano-sized catalysts. According to the London Metal Exchange, cobalt and palladium have a price ratio of approximately 1:750. According to their reactivities in catalyzing the model reaction of *p*-nitrophenol reduction by borohydride, the ratio of their mass-normalized reactivities is less than 1:1000 [1,2], suggesting a discouraging economic loss if cobalt is used to replace palladium to remediate *p*-nitrophenol.

The mass-normalized reactivity of nano-catalysts is directly correlated to their stability against aggregation [3]. To prevent aggregation, palladium nanoparticles have been prepared using a variety of stabilizing agents, including dendrimers [2], peptides [4], alumina (Al_2O_3) particles [5], and carbon nanotubes [6]. For the catalyzed reduction of *p*-nitrophenol by borohydride, the mass-normalized rate constants of palladium catalysts range over nearly 4 orders of magnitude from $k = 1.0$ to 6.9×10^3 min^{-1} g^{-1} L, with the most active palladium nanoparticles created under the stabilization of dendrimers [2,7]. In comparison, only limited efforts have been given to finding the appropriate stabilizers for nanoparticles made of non-precious metals such as cobalt. Examples of stabilizers for cobalt nanoparticles include reduced graphene oxide [8,9], hydrogel [10], and silica (SiO_2) cage [11], yielding $k = 0.82$–30.8 min^{-1} g^{-1} L in the catalyzed reduction of *p*-nitrophenol by borohydride. Compared to unsupported cobalt

* Corresponding author at: Department of Civil, Environmental, and Construction Engineering, 10th street and Akron Avenue, Lubbock, TX 79409.
E-mail address: chongzheng.na@gmail.com (C. Na).
[1] These authors contributed equally.

http://dx.doi.org/10.1016/j.apcatb.2015.06.052
0926-3373/

nanoparticles [12], only 2 orders of magnitude of improvement have been achieved using these stabilizing supports, much lower than the improvement made by stabilizing agents for palladium nano-catalysts.

Well-dispersed cobalt nanoparticles can be made by the topotactic transformation of layered double hydroxide (LDH) nanodisks [13]. LDH is a group of pseudo two-dimensional crystals having a structure similar to hydrotalcite ($Mg_6Al_2CO_3(OH)_{16}{\cdot}4(H_2O)$) [14]. This structure consists of alternating layers of metal oxides and intercalated water and anions. The disks often have a nominal diameter of micrometers but a thickness of only tens of nanometers. Cobalt has an ionic radius similar to that of magnesium; therefore, Co-containing LDH can be readily prepared by replacing part of magnesium with cobalt [15]. LDH is then calcined in the presence of hydrogen (H_2) gas above 600 °C, which separates Co from LDH and reduces it to the metallic nanoparticles [16]. The calcination also transforms LDH to layered double oxide (LDO) with a spinel ($MgAl_2O_4$) structure by removing intercalated water and carbonate anions [17]. Although spinel does not have a layered structure, because the platy morphology of LDH is largely preserved during calcination, the LDH derivative is often referred to as layered double oxide or LDO [18,19]. LDO-supported Co nanoparticles (LDO–Co) have been shown to be active in catalyzing hydrogenation reactions [20–23], steam reforming [24–30], aldol condensation [31], thermal decomposition [32,33], oxidation and combustion[34,35], and carbon nanotube synthesis [36–39].

LDH and the calcined derivative LDO have been previously investigated for water treatment and environmental remediation, utilizing their abilities of contaminant adsorption [40]. Here, we report the application of LDH-derived cobalt nano-catalysts for catalyzing the degradation of model contaminant *p*-nitrophenol. *p*-Nitrophenol is a Clean Water Act priority pollutant, which has an acceptable daily intake (ADI) of 0.32 mg per day over a month [41]. The toxicity of *p*-nitrophenol can be lowered significantly after it is reduced to *p*-aminophenol, which has a negligible ADI of 4.55 mg per day over lifetime [42]. We show that LDO–Co surpasses all the cobalt-based catalysts reported so far in the literature in catalyzing the reduction of *p*-nitrophenol by borohydride, giving a relative reactivity ratio of LDO–Co with the most active dendrimer-stabilized Pd nano-catalysts exceeding the price ratio of cobalt and palladium. Our results indicate that economic incentives exist for replacing palladium with cobalt in similar applications. Furthermore, we show that the high reactivity of LDO–Co retains with repeated use and is transferable when a more realistic hydrogen donor such as formate is used in place of borohydride. We propose that the reactivity and longevity of LDO-supported cobalt nanoparticles can be attributed to the superior stability resulting from heteroepitaxial fixation through interfacial Co-O bonds similar to those in spinel cobalt oxide.

2. Experimental section

Reagent-grade chemicals were purchased from Sigma–Aldrich except otherwise specified. Deionized (DI) water was generated on site using a Millipore system.

2.1. Preparation and characterization of LDO–Co

Urea ($CO(NH_2)_2$), aluminum nitrate ($Al(NO_3)_3$), magnesium nitrate ($Mg(NO_3)_2$), and cobalt nitrate ($Co(NO_3)_2$) were dissolved in 100 mL DI water, resulting in a urea concentration of 100 mM and a total metal concentration of 50 mM. The molar ratio of divalent magnesium and cobalt to trivalent aluminum was kept constant at 2:1. The molar percentage of cobalt with regard to all metals, θ, was varied from 0 to 67% (note: no Mg at $\theta = 67\%$).

LDH was synthesized in a sealed autoclave reactor at 100 °C in 12 h. LDH powder was collected by centrifugation, washed with DI water, and freeze–dried (Labconco Freezone 4.5). The powder was then placed inside a sealed quartz tubing and heated in a tube furnace to 600 °C under argon protection. Hydrogen was introduced into the quartz tubing at 50 sccm for 20 min to carry out thermal phase transformation. LDH, LDO, and LDO–Co were characterized using transmission electron microscopy (TEM; FEI Titan 300–80), scanning electron microscopy (SEM; FEI Magellan 400), atomic force microscopy (AFM; Park Systems XE 70), and powder X-ray diffraction (XRD; Bruker D8 Advance Davinci). Sample preparation and analyses were made following standard procedures. Metal contents in LDO–Co were measured using inductively coupled plasma optical emission spectroscopy (ICP-OES; PerkinElmer Optima 2000DV) after LDO–Co was completely digested in 70% nitric acid.

2.2. Catalytic reduction of p-nitrophenol by borohydride

A working suspension of LDO–Co was prepared by dispersing 2 mg LDO–Co in 8 mL DI water. The suspension was sonicated for 10 min to ensure complete dispersion. 0.75 mL working suspension was mixed with 32 mM $NaBH_4$ at a 1:1 volumetric ratio and shaken for 2 h to reduce any oxidized cobalt nanoparticles back to metallic cobalt. The mixture was then transferred into a standard UV/vis quartz cuvette. Another 1.5 mL $NaBH_4$ (32 mM) and 30 μL *p*-nitrophenol (20 mM) were added to the cuvette to initiate the *p*-nitrophenol reduction. The reaction solution was stirred with a small magnetic bar. The light absorption from 220 to 520 nm by the reactive solution was recorded every 30 s with a UV/vis spectrophotometer (Agilent Cary 300). A baseline absorbance was established using a 3-mL mixture consisting of LDO-Co and $NaBH_4$ but not *p*-nitrophenol. After subtracting the baseline, absorbance was converted to concentration using a calibration curve obtained with *p*-nitrophenol solutions of known concentrations.

2.3. Co nanoparticles loosely attached to LDO (LDO–Co*)

LDO–Co* was prepared in two steps. First, 20 mg LDO ($\theta = 0$) and 46.5 mg $Co(NO_3)_2{\cdot}9H_2O$ were added to 10 mL DI water under 10-min sonication and mixed on a shaking table for 24 h. LDO nanodisks with adsorbed Co^{2+} were then collected by centrifugation, washed with DI water for three times, and freeze–dried. Second, 12.5 mg LDO adsorbed with Co^{2+} was dispersed in 10 mL 32 mM $NaBH_4$ solution to reduce Co^{2+} to metallic Co. After 2 h, LDO–Co* was collected by centrifugation and used to catalyze the reduction of *p*-nitrophenol by borohydride. To do so, 1.5 mL suspension containing 1.25 g L^{-1} LDO–Co* was mixed with 1.5 mL $NaBH_4$ (32 mM) and 30 μL PNP (20 mM) in a quartz cuvette.

2.4. Catalytic reduction of p-nitrophenol by formate

The reaction was conducted in a 50-mL 3-neck flask immersed in water, which isolated contents inside the flask from air. 5 mg LDO–Co with $\theta = 28(\pm 2)\%$ was dispersed in 18.5 mL DI water by sonication and transferred into the flask. The solution was purged by N_2 at a flow rate of 60 sccm and mixed by a magnetic stir bar. The gas was released from the flask into air through a thin tubing. After 2 h, 1 mL DI water containing 10 mg $NaBH_4$ was added to reduce oxidized cobalt into metallic cobalt. After another 2 h, a mixture of 0.5 mL sodium formate (HCOONa, 2.0 M) and *p*-nitrophenol (8.0 mM) was injected into the flask to start the reaction. A control experiment was performed following the same protocol without adding sodium formate.

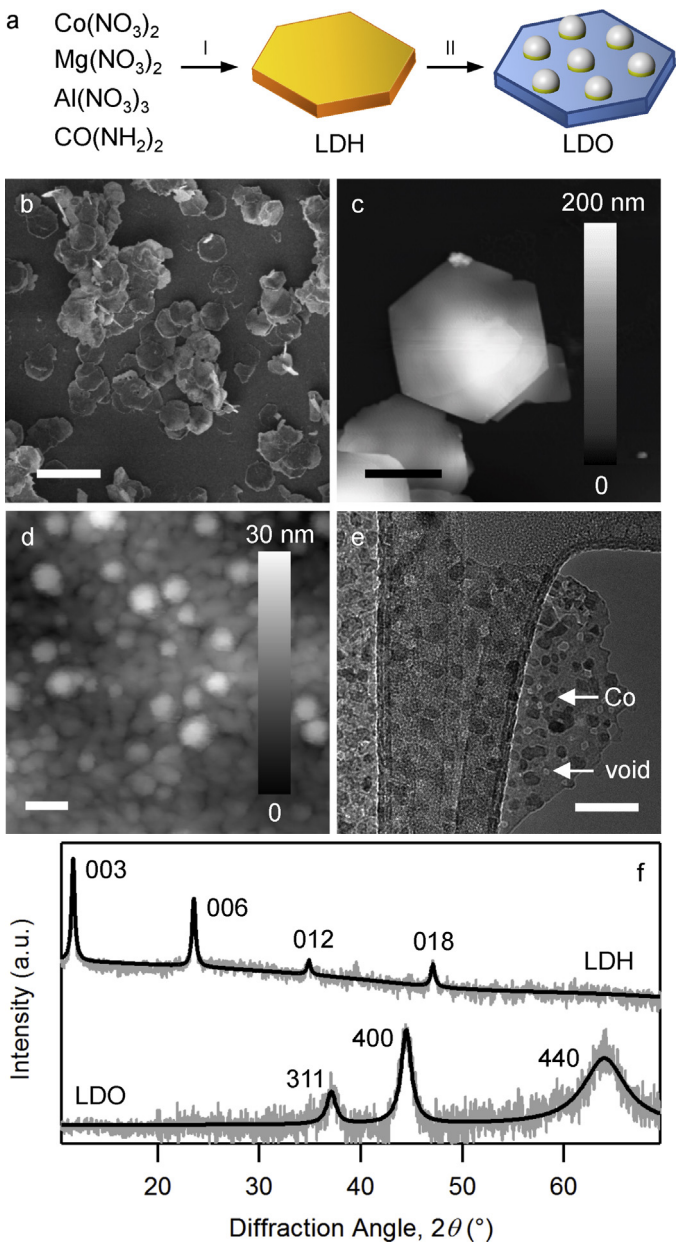

Fig. 1. Synthesis and characterization of layered double oxide (LDO)-supported cobalt nano-catalysts. (a) Schematic of critical steps: I. Hydrothermal synthesis of layered double hydroxide (LDH) and II. Conversion of LDH to nanoparticle-decorated LDO. (b) Scanning electron micrograph of LDH. (c, d) Atomic force micrographs of LDH and LDO nanodisks. (e) Transmission electron micrograph of cobalt-decorated LDO. (f) Powder X-ray diffraction patterns of LDH and LDO, reflections corresponding to hydrotalcite (JCPDS 70-2151) and spinel (JCPDS 21-1152) structures. Horizontal scale bars: *b*, 10 μm; *c*, 2 μm; *d* and *e*, 50 nm.

3. Results

3.1. Synthesis and characterization of LDO–Co

Cobalt nanoparticles supported on layered double oxide nanodisks are prepared by thermal phase transformation [6,29,30,43–45], involving two critical steps as illustrated in Fig. 1a [19,46–49]. First, layered double hydroxide nanodisks containing Co are synthesized by the hydrothermal reaction of cobalt, magnesium, and aluminum nitrates with urea. The hexagonal LDH nanodisks are approximately 4 μm in size and 45 nm in thickness, as shown in Fig. 1b and c. Second, LDH is annealed at 600 °C in hydrogen, creating nanoparticles affixedonthe nanodisks' surface, as shown in Fig. 1d and e. AFM measurements, as illustrated in Fig. 1d, show that the nanoparticles have heights comparable to their diameters, suggesting that the nanoparticles are pseudo-spherical. TEM reveals voids inside the nanodisks, as marked in Fig. 1e, possibly formed by the loss of water and intercalated carbonic acid during annealing (cf. Fig. S1 for no voids in LDH). XRD confirms that LDH has a hydrotalcite structure [14], as shown in Fig. 1f. The XRD peaks for LDH are sharp, suggesting a LDH crystal can be as large as a single disk with micrometers in size. XRD also reveals that annealing transforms LDH to a spinel oxide structure [50,51] while the nanodisks' platy morphology is preserved (Fig. S2). The wide XRD peaks observed for LDO confirms that LDO is made of nanometer-sized crystallites [52], consistent with the presence of nanometer-sized voids inside the platy nanodisks. The voids have hexagonal shapes, consistent with the closely packed lattices of brucite planes in hydrotalcite [6]. For LDO–Co, cobalt nanoparticles represent a minority component and, thus are not resolved by XRD.

We further investigate the morphology and phases of LDO–Co using high-resolution TEM. Three crystalline phases, Co-HCP, Co_3O_4 and $MgAl_2O_4$ are identified in the samples. Cobalt oxide is formed when LDO–Co is removed from the reducing environment where it is synthesized under argon protection. The oxidation of cobalt transition metal nanoparticles in the air is not exceptional because most transition metal nanoparticles except those of noble metals are readily oxidized when they are exposed to air. In practice, oxidation is not expected to be an issue when LDO–Co is continuously used in a reducing environment. When cobalt is oxidized due to exposure to an oxidizing environment such as the air, it can be readily reduced back to the metallic state using agents such as borohydride.

As shown in Fig. 2a–c, Co nanoparticles exposed in the air for half an hour between sample preparation and examination have a core-shell structure. Fast Fourier transform (FFT) of the TEM reveals that the cobalt core has a hexagonal close packing (HCP) structure, consistent with the phase diagram of cobalt under 600 °C [53]. With LDO–Co lying flat on the TEM grid, Co-HCP is viewed in the [001] direction, suggesting that the closely packed {0 0 1} plane of Co-HCP is in parallel with the LDO surface. The shell consists of Co oxides as a result of accelerated oxidation of Co nanoparticles at the nanometer scale [54] according to the Cabrera-Mott mechanism [55]. After being exposed in the air for 2 days, the nanoparticles are completely oxidized to cobalt oxide Co_3O_4, as shown in Fig. 2d–f. The identification of Co_3O_4 is facilitated by FFT, showing a spinel structure viewed along the [1 1 1] zone axis. This orientation also suggests that the closely packed {1 1 1} plane of Co_3O_4 is parallel to the LDO surface. Similar to Co_3O_4, LDO also has a spinel structure, shown in Fig. 2g–i. The FFT pattern of LDO further shows that from the top, LDO is viewed along the [1 1 1] zone axis, indicating thatits surface is formed by the closely packed {1 1 1} plane.

We measure the diameter d_o of completely oxidized nanoparticles and estimate the diameter d of cobalt nanoparticles by assuming the elimination of all oxygen after borohydride reduction (i.e., $d = 0.51d_o$). For each sample, measurements show that the values of d are normally distributed (Fig. S3), which can be represented by the mean in combination with the standard deviation. With cobalt molar percentage $\theta = 0$–$28(\pm2)\%$ as measured by ICP-OES after acid digestion, d can be varied from 0 to $11.1(\pm4.9)$ nm (standard deviation in parentheses), as shown in Fig. 3a. The increase of d with θ is found to follow $d = 3.8(\pm0.1)\theta^{1/3}$ ($R^2 = 0.99$), suggesting that the nanoparticles have increased in size but not in density. However, at $\theta > 28(\pm2)\%$, the boundaries between nanoparticles are no longer discernible, as shown in Fig. 3b, suggesting the formation of a continuous cobalt film.

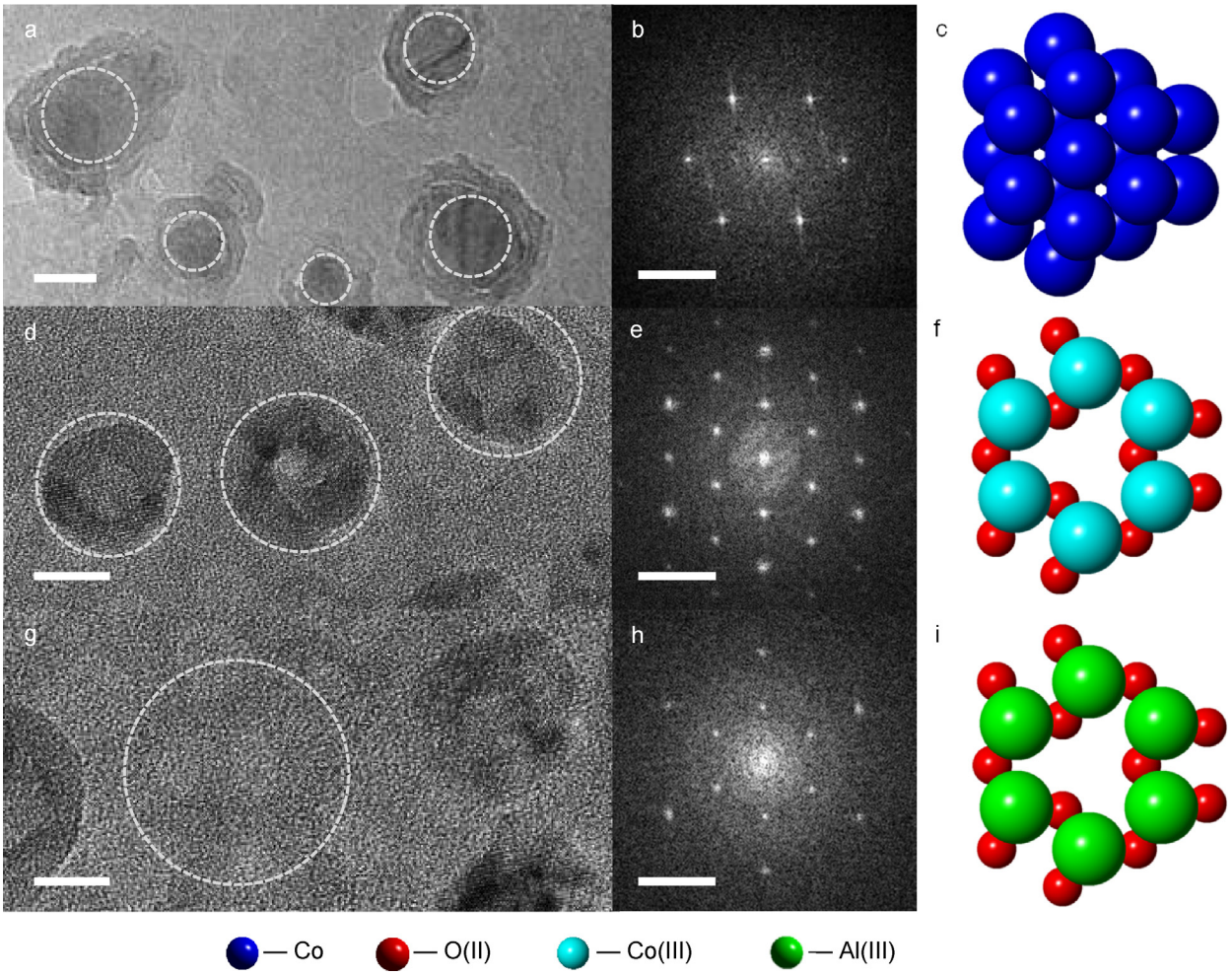

Fig. 2. Cobalt and cobalt oxide nanoparticles affixed on layered double oxide (LDO) nanodisks. (a, b, c) High-resolution transmission micrographs (HRTEM), fast Fourier transformation (FFT), and molecular model of the metallic core for partially oxidized nanoparticles. (d, e, f) HRTEM, FFT, and molecular model of cobalt oxide (Co_3O_4) for completely oxidized cobalt nanoparticles. (g, h, i) HRTEM, FFT, and molecular model of the LDO support. White circles mark the areas in HRTEM where FFT analyses are performed. Sample orientation [direction perpendicular to paper, direction pointing upward within paper]: Co, [001, 010]; Co_3O_4, [111, 01$\bar{1}$]; LDO, [111, 01$\bar{1}$]. Scale bars: *a*, *d*, *g*, 10 nm; *b*, *e*, *h*, 5 nm^{-1}.

3.2. *Reactivity of LDO–Co in catalyzing* p*-nitrophenol reduction by borohydride*

We demonstrate the high catalytic reactivity of LDO–Co using the model reaction of *p*-nitrophenol reduction by borohydride. This reaction is selected partly because of its well-understood reaction mechanism and easy-to-follow kinetics [56]. In the presence of metal catalysts, the nitro group of *p*-nitrophenol is transformed to the amino group by borohydride, as shown in Fig. 4a. The change of *p*-nitrophenol concentration can be quantified using the absorbance at 400 nm according to Beer's law [57].

To ensure all the nanoparticles are in the metallic state, LDO–Co is reacted with borohydride for 2 h before being used for catalysis. After 2 h, an excess amount of borohydride (final concentration:

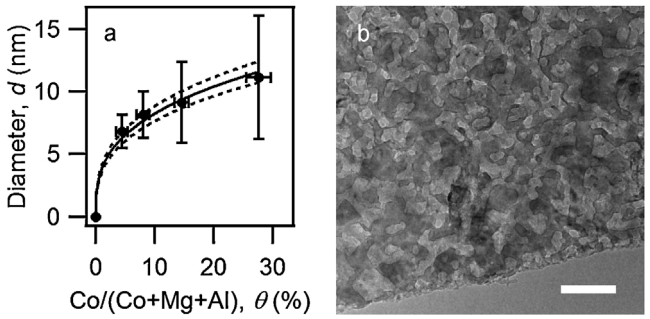

Fig. 3. Dependence of nanoparticle size oncobalt molar percentage (θ). (a) Increase of the diameter of Co nanoparticles with θ = Co/(Co + Al + Mg). (b) Continuous film formed at θ = 51%. The solid and dashed curves in *a* are the least-squares fit and 90% confidence intervals of $d = \chi\theta^{1/3}$ (R^2 = 0.99). Scale bars: 50 nm.

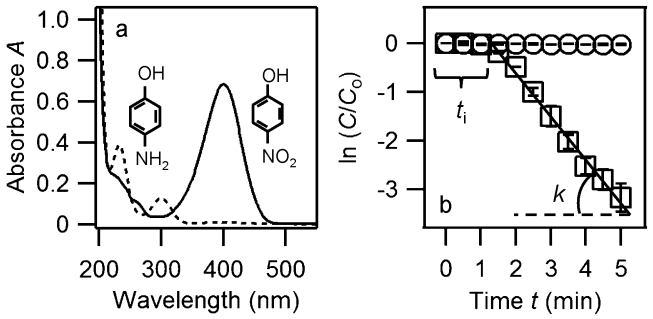

Fig. 4. Catalytic reactivity of LDO-supported cobalt nanoparticles. (a) Reduction of *p*-nitrophenol (solid curve) to *p*-aminophenol (dashed curve). (b) Pseudo first order kinetics with an induction time (squares: with LDO–Co; circles: without LDO–Co). The line is a linear fit to Equation (1). LDO–Co: Co molar percentage, 15(±1)%.

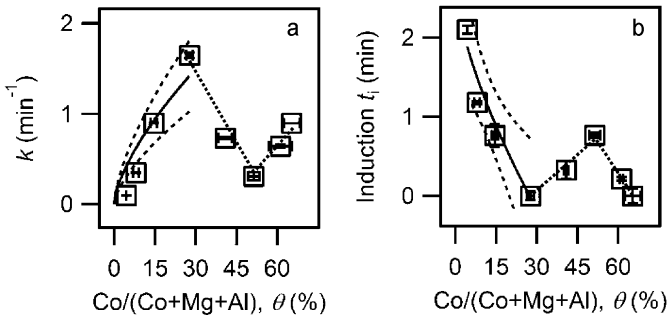

Fig. 5. Dependence of (a) pseudo first order rate constant and (b) induction timeon cobalt molar percentage. The solid curves are least-square regressions of k and t_i to $\theta^{2/3}$ (R^2 = 0.95 and 0.99) for $\theta \leq 28\%$. The dashed lines brackets 90% confidence intervals. The dotted lines connect the remaining data points.

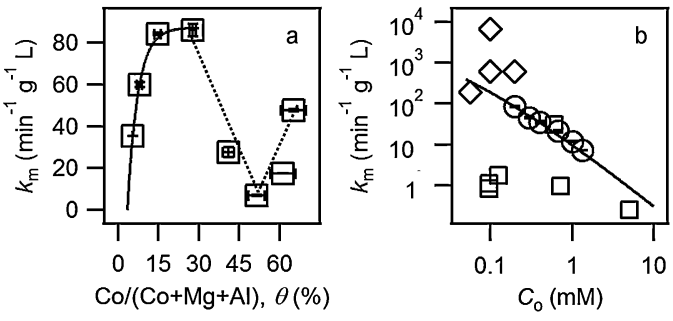

Fig. 6. Mass-averaged pseudo first order rate constant (k_m) of LDO–Co-catalyzed reduction of *p*-nitrophenol by borohydride. (a) Dependence of k_m on cobalt molar percentage θ. (b) Comparisons of k_m values for LDO–Co (circles) with those for other cobalt catalysts (squares) and various support-stabilized palladium nanoparticles (diamonds), as a function of initial *p*-nitrophenol concentration C_o. The solid curves in *a* and *b* are least-squares fits to the exponential function (R^2 = 0.97) and the Langmuir-Hinshelwood model of Equation (2) (R^2 = 0.98), respectively. The dash lines in *a* are linear fits. See Table S1 for literature data used to generate *b*.

16 mM) is added together with *p*-nitrophenol (0.2 mM) to initiate the catalyzed reduction. The excess amount of borohydride is used to facilitate comparisons of LDO–Co reactivity because the reactivities of most cobalt and palladium-based catalysts reported in the literature are measured under similar conditions. It is worth noting that the mechanism of catalyzed reduction of *p*-nitrophenol by borohydride, including the dependence of reaction kinetics on borohydride concentration, is well understood [56]. Hence, the elucidation of the reaction mechanism is not the focus of this study.

Once *p*-nitrophenol is mixed with LDO–Co and an excess amount of borohydride, its concentration begins to decrease rapidly. As shown by the squares in Fig. 4b, *p*-nitrophenol reduction conforms to a pseudo first order rate law after an induction period t_i:

$$\ln(C/C_o) = -k(t-t_i) \quad (1)$$

where C_o and C are initial and residual *p*-nitrophenol concentrations, t is the reaction time, and k is the rate constant. In comparison, $\ln(C/C_o)$ does not show discernible change with t when borohydride is added in the absence of LDO–Co (circles in Fig. 4b). k and t_i are estimated from the intercept and slope of the linearity between $\ln(C/C_o)$ and t. A linear correlation is observed between k and the concentration of LDO–Co (Fig. S4), confirming that the reaction is not limited by mass transfer.

k shows a complex relationship with θ, as depicted in Fig. 5a. For $0 \leq \theta \leq 28\%$, k increases monotonically with θ, following a linear correlation between k and $\theta^{2/3}$ (R^2 = 0.95). At θ = 0, a negligible value of $k = 0.003(\pm 0.001)\,\text{min}^{-1}$ is estimated from the control sample shown by the circles in Fig. 4b. Considering that d increases with $\theta^{1/3}$ (Fig. 3a), the correlation between k and $\theta^{2/3}$ suggests that the increase of total surface area is responsible for the increase of k in this θ range. As θ further increases, k decreases corresponding to the formation of a continuous cobalt film (cf. Fig. 3b), which eliminates most of the reactive edge and corner sites and thus reduces the overall catalytic reactivity of LDO–Co. Further increase of θ from 51% to 67% leads to an increase of k, possibly due to the formation of new nanoparticles on top of the continuous film.

The relationship between t_i and θ exhibits a complete inversion of the k–θ relationship, as shown in Fig. 5b. This relationship can be explained by considering the adsorption of *p*-nitrophenol and borohydride at the beginning of the reaction. It is well established that the catalytic reduction of *p*-nitrophenol by borohydride follows the Langmuir–Hinshelwood mechanism [56,58], which involves two steps, including (1) dissociative adsorption of both reactants on the catalyst surface and (2) reaction between adsorbed species. Since LDO–Co has been in contact with borohydride for 2 h before the addition of *p*-nitrophenol, the species controlling reaction kinetics is *p*-nitrophenol. At the beginning of the reaction, the surface concentration of *p*-nitrophenol is increased from zero to the steady-state concentration through adsorption. This process takes time, as reflected by the presence of t_i. According to the Langmuir kinetics [8], t_i is inversely related to the catalyst's total surface area or d^2 for LDO–Co. Since $d \propto \theta^{1/3}$, we expect $t_i \propto \theta^{2/3}$ for $0 \leq \theta \leq 28\%$, as shown in Fig. 5b. As θ increases to 51% and then to 67%, t_i first increases and then decreases, following the inverse trends of surface area change.

3.3. Comparisons with previous Co and Pd nano-catalysts

Fig. 6a shows the dependence of LDO–Co reactivity on θ after k is normalized to the cobalt loading of LDO–Co. The maximum mass-normalized rate constant k_m is found with θ = 28% at $k_m = 86(\pm 3)\,\text{min}^{-1}\,\text{g}^{-1}\,\text{L}$ for C_o = 0.2 mM. According to a semi-empirical Langmuir–Hinshelwood model [56], k_m is a function of the initial *p*-nitrophenol concentration C_o:

$$k_m = \frac{k_{rxn} S K_{PNP} K_{BH_4^-} C_{BH_4^-}}{C_o^{0.4}\left(1 + K_{PNP}^{0.6} C_o^{0.6} + K_{BH_4^-} C_{BH_4^-}\right)^2} \quad (2)$$

where k_{rxn} is the reaction rate constant for adsorbed *p*-nitrophenol and borohydride, S is the active site density, K_{PNP} and $K_{BH_4^-}$ are adsorption constants for *p*-nitrophenol (PNP) and borohydride, and $C_{BH_4^-}$ is the concentration of borohydride. Indeed, we observe a decrease of k_m with increasing C_o due to the increasing competition of *p*-nitrophenol with borohydride for adsorption, as shown by the circles and the solid curve in Fig. 6b.

In comparison to suspended cobalt nano-catalysts [1,12] and cobalt nanoparticles supported on reduced graphene oxide [8,9] and hydrogel [10], LDO–Co exhibits a clear improvement in catalytic activity (cf. Table S1). For measurements made with an initial *p*-nitrophenol concentration of 0.1–0.2 mM, the reactivity of LDO–Co shows 49 times improvement compared to the highest reactivity obtained with previously reported Co nano-catalysts (i.e., $Co(OH)_2$ nanosheets) [12]. At C_o = 0.6 mM, cobalt nanoparticles secured in silica cages ($Co@SiO_2$) [11] show similar reactivity as LDO–Co, as marked by the square near to the solid curve in Fig. 6. However, the reactivity of $Co@SiO_2$ deteriorates rapidly with reuse whereas the reactivity of LDO–Co remains unchanged with reuse (see below). In addition, the reactivity of LDO–Co has surpassed the reactivities of Co-based alloys (highest reported rate: $6.4\,\text{min}^{-1}\,\text{g}^{-1}\,\text{L}$) [59–61].

Compared to the highly reactive dendrimer-stabilized Pd catalyst (the highest diamond symbol in Fig. 6) [2,4,5], LDO–Co gives a relative reactivity ratio of k_m(LDO–Co)/k_m(dendrimer-Pd) = 1:80. This ratio is 9.3 times the price ratio of 1:750 between cobalt

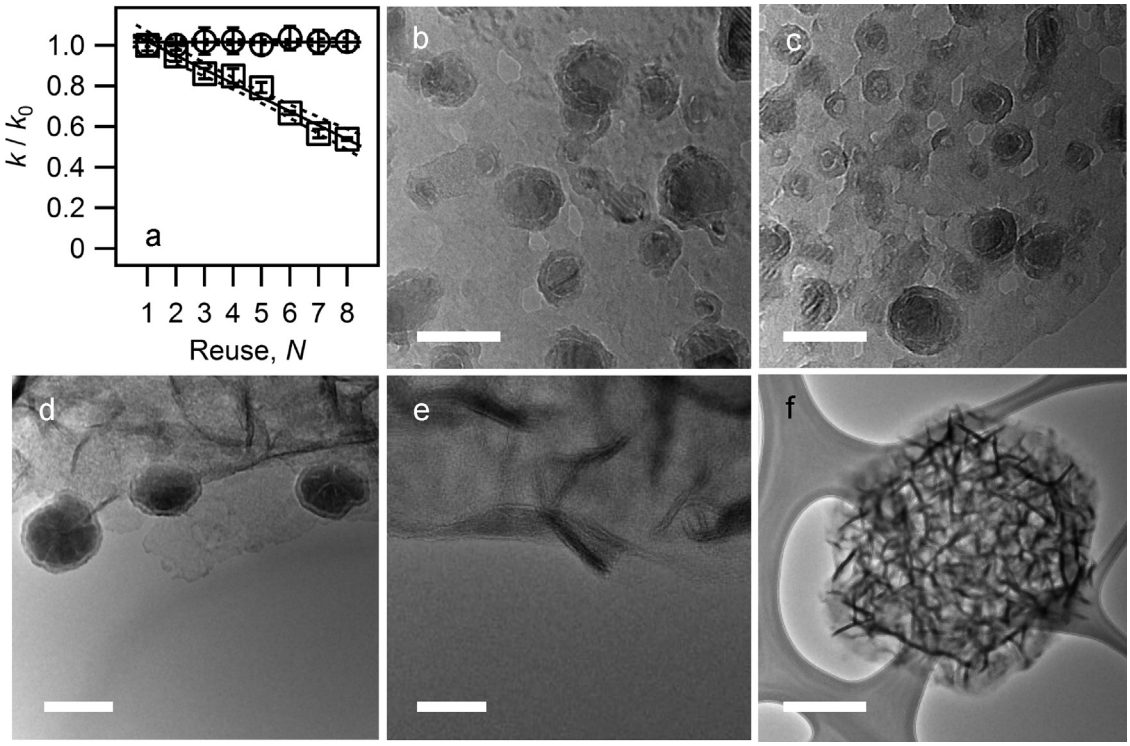

Fig. 7. Prevention of nanoparticle aggregation by affixing cobalt nanoparticles on LDO via thermal phase transformation. (a) Comparison of reactivity, as expressed in the ratio of the rate constant obtained from *p*-nitrophenol reduction in each reuse to the rate constant obtained in the pristine use (k/k_0), between cobalt affixed on LDO (LDO–Co; circles) and cobalt loosely attached to LDO (LDO–Co*; squares). (b, c) Transmission electron micrographs (TEMs) of LDO–Co before and after reaction. (d) TEM of LDO–Co* before reaction. (e, f) TEM of LDO–Co* after reaction. Scale bars: *b* and *c*, 20 nm; *d* and *e*, 40 nm; *f*, 500 nm.

and palladium. The direct comparison of catalyst reactivity and metal price is certainly an oversimplification regarding the costs of catalytic water treatment. Nonetheless, our results suggest that a financial gain may be made by replacing palladium-based nanocatalysts with LDO–Co and thus, further investigation is warranted.

3.4. Stability of LDO–Co in reuse

To investigate the longevity of LDO–Co during extended use, LDO–Co nanodisks are separated at the end of an experiment using magnetic attraction. The collected LDO–Co is then re-dispersed in a mixture of *p*-nitrophenol and borohydride to be evaluated for reuse. As shown in Fig. 7a, the ratio of *k* obtained in each reuse to the rate constant obtained with the pristine sample (k/k_0) varies little with repeated use, confirming the successful prevention of nanoparticle aggregation by affixing cobalt nanoparticles on LDO. This is consistent with comparisons made by TEM before and after reaction, as shown in Fig. 7b and c, revealing that nanoparticles are similarly distributed on the LDO surface with no discernible aggregation. In addition to the stability of cobalt nanoparticles, the LDO support is also structurally stable, as evident from the similar XRD spectra measured before and after reaction (Fig. S5).

We propose that the affixation of cobalt nanoparticles on LDO by thermal phase transformation is essential for the longevity of LDO–Co. To examine this hypothesis, we have synthesized a control sample with Co nanoparticles only loosely attached to the LDO surface, which we refer to as LDO–Co*. LDO–Co* is synthesized by adsorbing Co^{2+} on LDO from an aqueous solution and reducing it to metallic cobalt in a borohydride solution. As shown in Fig. 7d, this method produces cobalt nanoparticles having diameters around 37(±6) nm. In addition to the size difference, most of the nanoparticles in LDO–Co* are attached to the edges of LDO nanodisks in contrast to the nanoparticles well-dispersed on LDO–Co surfaces. The cobalt content in LDO–Co* is estimated at 16.2% by ICP-OES after acid digestion. When pristine LDO–Co* is used to catalyze the reduction of *p*-nitrophenol by borohydride, a pseudo first order rate law is also observed, giving a rate constant of $k_0 = 9.4\ min^{-1}\ g^{-1}\ L$. This value is approximately an order of magnitude lower than that for LDO–Co with the same cobalt content (i.e., $\theta = 16.2\%$). The reduced reactivity can be attributed to the large size of cobalt nanoparticles in LDO–Co* compared to those in LDO–Co (37 vs 9.7 nm, respectively). In addition, the reactivity of LDO–Co* keeps decreasing linearly after repeated use, as shown by the squares in Fig. 7a. The decrease of *k* follows a reduction rate of 7(±1)% per use and reaches 46% after the 8th use. TEM examination of LDO–Co* after reuse reveals that few cobalt nanoparticles can still be found on LDO, as shown in Fig. 7e and f, suggesting that the loosely attached nanoparticles have fallen off the support and possibly have aggregated in solution.

3.5. Catalytic activity of LDO–Co with formate as hydrogen donor

Although sodium borohydride has been widely used in both scientific investigations [58,62,63] and industrial applications [64–68], the application of borohydride in remediation is still challenging. As a strong reductant, borohydride reacts with water in the absence of catalysts, although much slower, and thus can lose reactivity over time. The use of borohydride introduces boron, in the form of borate as the oxidation product of borohydride, into the receiving water body, which may pose health concerns. In comparison, formate is a moderate reductant and hydrogen donor. Formate has been shown to reduce nitrophenol under the catalysis of palladium [69]; however, the reduction of nitrophenol by formate has not been investigated for non-precious metal catalysts including cobalt.

To investigate whether LDO–Co can catalyze the reduction of *p*-nitrophenol by formate, we measure the change of *p*-nitrophenol concentration in a mixture with sodium formate with and without LDO–Co. As shown in Fig. 8, the reduction of *p*-nitrophenol by formate has a negligible rate in the absence of LDO–Co. In the presence of LDO–Co, the reduction follows a pseudo first order rate law. The rate constant is estimated at $k = 0.36\ (\pm 0.01)\ \mathrm{min^{-1}\ g^{-1}\ L}$ with a LDO–Co concentration of $0.1\ \mathrm{g\,L^{-1}}$, an initial *p*-nitrophenol concentration of 0.2 mM, and an initial formate concentration of 50 mM (only 3.125 times the typical borohydride concentration). Although this rate constant is 239 times smaller than the rate constant obtained using borohydride, it should be considered evidence of LDO–Co being highly reactive with formate as the hydrogen donor because it gives a relative reactivity ratio of 1:13 with palladium [69].

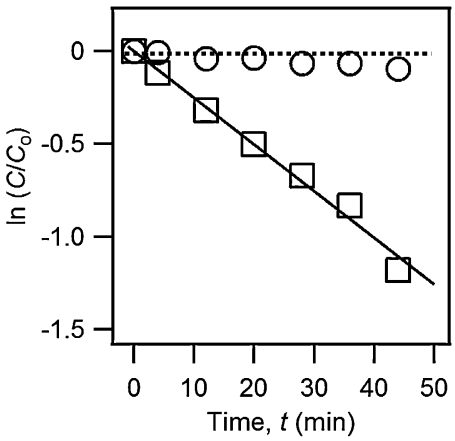

Fig. 8. Reduction of *p*-nitrophenol by formate catalyzed by LDO-supported cobalt nanoparticles. Symbols: circles, no LDO–Co; squares, LDO–Co. The solid line is a linear fit to Equation (1). The horizontal dash line represents an average. Experimental conditions: LDO–Co, $0.1\ \mathrm{g\,L^{-1}}$; cobalt molar percentage, 28%; nanoparticle diameter, 11.1(±4.9) nm; *p*-nitrophenol, 0.2 mM; sodium formate, 50 mM.

4. Discussion

Our results show that cobalt nanoparticles synthesized by thermal phase transformation are tightly fixed on LDO supports. The immobilization of cobalt nanoparticles is essential for their initial

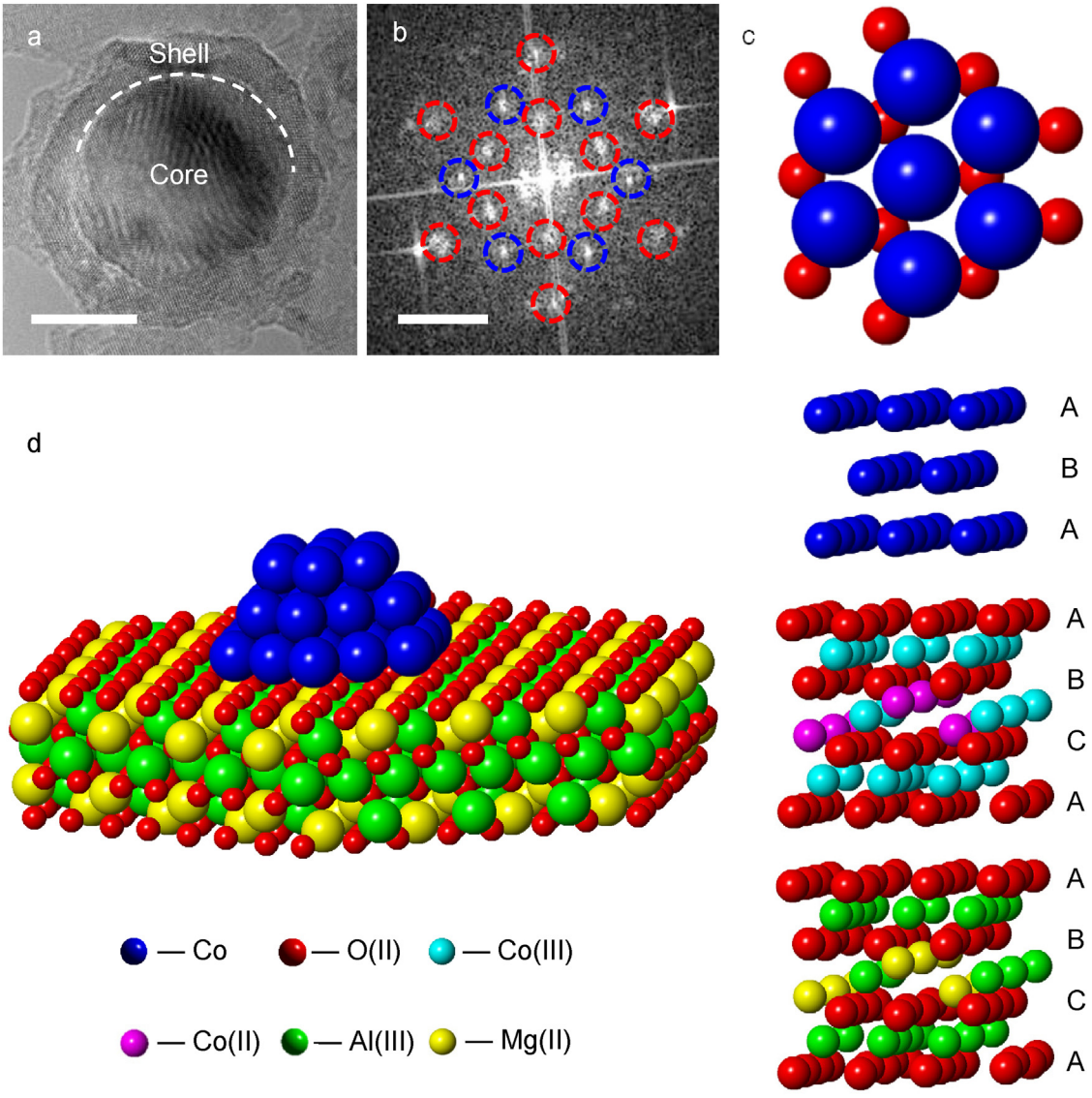

Fig. 9. Heteroepitaxial fixation of cobalt nanoparticles on the spinel LDO support. (a, b, c) Transmission electron micrograph, fast Fourier transformation, and molecular model of a $Co@Co_3O_4$ core-shell nanoparticle on top of LDO. (d) Molecular model of heteroepitaxial stacking. Scale bar: *a*, 10 nm.

and sustained high reactivity in catalysis. Because cobalt is readily oxidized by oxygen in the air, nanoparticles supported on LDO are observed as a Co@Co_3O_4 core-shell structure. A comprehensive survey of the LDO–Co samples prepared in this study reveals that Co@Co_3O_4 nanoparticlesare not randomly stacked on top of the LDO surface. As shown in Fig. 9a–c, the FFT of the core-shell gives two sets of electron diffraction patterns that match exactly those of Co-HCP and $MgAl_2O_4$ (cf. Fig. 2b and h). The direction perpendicular to the LDO surface overlaps with the [0 0 1] zone axis of Co-HCP and the [1 1 1] zone axis of $MgAl_2O_4$, suggesting that within the surface plane, Co-HCP [010] is aligned with $MgAl_2O_4$ [01$\bar{1}$] (i.e., the direction pointing upward). Since there is no unassigned diffraction spot left, the pattern created by Co_3O_4 must have overlapped with the pattern created by spinel LDO.

The deconvolution of the FFT patternsgenerated by LDO-supported Co@Co_3O_4 suggests that the nanoparticles are affixed on LDO by heteroepitaxy. As shown in Fig. 9d, the structure of Co-HCP can be viewed as the stacking of two {0 0 1} layers of closely packed Co atoms (marked as A and B) [70]. The spinel structures of Co_3O_4 and $MgAl_2O_4$ can be envisioned as the stacking of three different layers of cubic-close packed O anions (marked as A, B, and C) [71]. Oxygen atoms in A and B layers form octahedrons with centers occupied by Co(III) cations. Oxygen atoms in B and C layers form alternating octahedrons and tetrahedrons with centers occupied by Co(III) and Co(II) cations, respectively. The unique orientations of Co-HCP and LDO, as elucidated in Fig. 9a–c, place six out of every seven hexagonally packed cobalt atoms in the {0 0 1} facet on top of the O atoms in the {1 1 1} facet of $MgAl_2O_4$. Each of the six cobalt atoms can then form three Co—O bonds with the underlying O atoms similar to Co(III) in Co_3O_4.

The hypothesis that Co@Co_3O_4 nanoparticles are affixed on LDO through heteroepitaxy is supported by the similarity between the length of Co—Co bonds in Co—HCP and the length of Co(III)—Co(III) bonds in Co_3O_4. For bulk Co—HCP, the Co—Co bond has a length of 0.251 nm. In comparison, the length of Co(III)—Co(III) in Co_3O_4 is 0.286 nm, suggesting that Co—Co bonds in Co—HCP only needs to stretch 14% to replace Co(III) on the surface of LDO. Similar degrees of mismatch has been observed on the heteroepitaxial growth of FeO(1 1 1) and Fe_3O_4(1 1 1) on Pt(1 1 1) [72]; therefore, the degree of bond stretching required for the formation interfacial Co(III)—O bonds between Co—HCP and LDO is reasonable and should not lead to the disintegration of cobalt nanoparticles. On the contrary, the lateral stretching of Co—Co distance may assist the accommodation of the seventh cobalt atom located in the center of the hexagon that is not bonded to LDO oxygen underneath. Although we cannot perform microscopic examination of the supported nanoparticles in the pure metallic state due to the oxidation of metallic cobalt by oxygen in the air, the unfaltering reactivity of LDO–Co in reuse suggests that the interfacial Co—O bonds are intact even after Co_3O_4 is reduced to Co—HCP by borohydride.

To catalyze reductive reactions, transition metal nanoparticles that have been oxidized by ambient oxygen need to be reduced back to the metallic state for activation. For LDO–Co, the reductive activation can be performed by borohydride in situ. Although the reduction potential of Co_3O_4 to metallic Co has not been reported, the fact that Co can be oxidized under the ambient condition suggests that $E(Co_3O_4/Co) < E(O_2/H_2O;\ pH\ 7) = 0.82$ V [73]. Borohydride is a potent reductant with a potential of $E(BO_2^-/BH_4^-) < -1.0$ V under our experimental conditions (i.e., ca. pH 10–11). The presence of Co core observed under TEM supports the reduction of Co_3O_4 to metallic Co by borohydride (cf. Fig. 2). Previously, cobalt boride (Co_2B) was claimed as a product of the reduction of Co_3O_4 by borohydride [74]; however, it has been contended that the sole experimental evidence obtained from XRD was insufficient to support the identification of the boride phase [75]. In our analyses, we find no evidence suggesting the formation of cobalt boride. Whether boron is present at the surface of LDO–Co during the reduction of PNP is, however, beyond the scope of this study.

5. Conclusions

We have successfully synthesized LDO-supported cobalt nanoparticles from Co—Mg—Al hydrotalcite by thermal phase transformation. We have shown that the catalytic reactivity of cobalt nanoparticles is greatly improved by affixing them on LDO nanodisks through heteroepitaxy to resist aggregation. Compared to cobalt nano-catalysts reported previously, LDO–Co exhibits at least 49 times increase in mass-normalized reactivity for catalyzing the reduction of *p*-nitrophenol by borohydride. This has greatly reduced the difference between the catalytic reactivity of cobalt and that of dendrimer-stabilized palladium, the best precious metal catalyst for *p*-nitrophenol reduction. This encouraging result supports further development of sustainable non-precious metal catalysts for water and wastewater treatment.

It is worth noting that synthesizing cobalt nanoparticles with diameters around and under 10 nm is still challenging even when stabilizing surfactants such as poly(vinyl pyrrolidone) are used in synthesis [76,77]. The ability to synthesize exposed cobalt nanoparticles in this size range is particularly advantageous because although stabilizing surfactants can help control nanoparticle size and shape [78], they can also block the access to active surface sites and lead to reduced reactivity [79]. For this reason, surfactant-free nanoparticles such as those supported on LDO are highly desirable.

Compared to LDO–Co, there is no report for preparing LDO-Pd by the thermal phase transformation of Pd-containing LDH. Different from Co-containing LDH in which cobalt is incorporated in the brucite layers by replacing magnesium, anion-coordinated palladium cations are intercalated between the brucite layers [80,81], which may interfere with the phase transformation process. Palladium nanoparticles can be attached on LDH or LDO surfaces by adsorption with or without the use of polymer linkers; however, this method of direct decoration is unlikely to result in an improvement of reactivity compared to well-dispersed dendrimer-stabilized palladium nanoparticles because the nanoparticles created by the direct decoration method can only create loosely attached nanoparticles [70] that can still fall off the support and aggregate.

Acknowledgements

We thank financial support from the DOE Office of Nuclear Energy's Nuclear Energy University Programs, the National Science Foundation's Environmental Engineering Program, and the University of Notre Dame Sustainable Energy Initiative. H.M. also acknowledges support from the Bayer Predoctoral Research Fellowship provided by the Notre Dame Center for Environmental Science and Technology.

Appendix A. Supplementary data

Supplementary data associated with this article can be found, in the online version, at http://dx.doi.org/10.1016/j.apcatb.2015.06.052

References

[1] J.M. Song, J.J. Ni, J. Zhang, D. Ling, H.L. Niu, C.J. Mao, S.Y. Zhang, Y.H. Shen, J. Nanopart. Res. 16 (2014) 2269.
[2] Y. Mei, Y. Lu, F. Polzer, M. Ballauff, M. Drechsler, Chem. Mater. 19 (2007) 1062–1069.
[3] S. Özkar, R.G. Finke, J. Am. Chem. Soc. 124 (2002) 5796–5810.
[4] R. Bhandari, M.R. Knecht, ACS Catal. 1 (2011) 89–98.
[5] S. Arora, P. Kapoor, M.L. Singla, React. Kinet. Mech. Cat. 99 (2010) 157–165.

[6] H. Wang, H. Ma, W. Zheng, D. An, C. Na, ACS Appl. Mater. Interfaces 6 (2014) 9426–9434.
[7] A. Halder, S. Patra, B. Viswanath, N. Munichandraiah, N. Ravishankar, Nanoscale 3 (2011) 725–730.
[8] F.J. Chen, P.X. Xi, C. Ma, C.W. Shao, J. Wang, S. Wang, G.Z. Liu, Z.Z. Zeng, Dalton Trans. 42 (2013) 7936–7942.
[9] S. Bai, X.P. Shen, G.X. Zhu, M.Z. Li, H.T. Xi, K.M. Chen, ACS Appl Mater. Interfaces 4 (2012) 2378–2386.
[10] N. Sahiner, H. Ozay, O. Ozay, N. Aktas, Appl. Catal. B 101 (2010) 137–143.
[11] N. Yan, Z. Zhao, Y. Li, F. Wang, H. Zhong, Q. Chen, Inorg. Chem. 53 (2014) 9073–9079.
[12] T.R. Mandlimath, B. Gopal, J. Mol. Catal. A: Chem. 350 (2011) 9–15.
[13] F. Cavani, F. Trifiro, A. Vaccari, Catal. Today 11 (1991) 173–301.
[14] M. Bellotto, B. Rebours, O. Clause, J. Lynch, D. Bazin, E. Elkaim, J. Phys. Chem. 100 (1996) 8527–8534.
[15] W.T. Reichle, Solid State Ionics 22 (1986) 135–141.
[16] W.T. Reichle, J. Catal. 94 (1985) 547–557.
[17] S. Ribet, D. Tichit, B. Coq, B. Ducourant, F. Morato, J. Solid State Chem. 142 (1999) 382–392.
[18] S. Carlino, Solid State Ionics 98 (1997) 73–84.
[19] M.J. Hudson, S. Carlino, D.C. Apperley, J. Mater. Chem. 5 (1995) 323–329.
[20] B. Coq, D. Tichit, S. Ribet, J. Catal. 189 (2000) 117–128.
[21] Y.-T. Tsai, X. Mo, A. Campos, J.G. Goodwin Jr., J.J. Spivey, Appl. Catal. 396 (2011) 91–100.
[22] A.E. Palomares, J.M. López-Nieto, F.J. Lázaro, A. López, A. Corma, Appl. Catal. B 20 (1999) 257–266.
[23] A. Di Fronzo, C. Pirola, A. Comazzi, F. Galli, C.L. Bianchi, A. Di Michele, R. Vivani, M. Nocchetti, M. Bastianini, D.C. Boffito, Fuel 119 (2014) 62–69.
[24] L. Wang, D. Li, H. Watanabe, M. Tamura, Y. Nakagawa, K. Tomishige, Appl. Catal. B 150–151 (2014) 82–92.
[25] J.S. Moura, M.O.G. Souza, J.D.A. Bellido, E.M. Assaf, M. Opportus, P. Reyes, M.D.C. Rangel, Int. J. Hydrog. Energy 37 (2012) 3213–3224.
[26] R. Espinal, E. Taboada, E. Molins, R. Chimentao, F. Medina, J. Llorca, Top. Catal. 56 (2013) 1660–1671.
[27] G. Garbarino, P. Riani, M.A. Lucchini, F. Canepa, S. Kawale, G. Busca, Int. J. Hydrog. Energy 38 (2013) 82–91.
[28] L.Y. Dolgykh, I.L. Stolyarchuk, I.V. Vasylenko, Y.I. Pyatnitsky, P.E. Strizhak, Theor. Exp. Chem. 49 (2013) 185–192.
[29] R. Espinal, E. Taboada, E. Molins, R.J. Chimentao, F. Medina, J. Llorca, RSC Adv. 2 (2012) 2946–2956.
[30] R. Espinal, E. Taboada, E. Molins, R.J. Chimentao, F. Medina, J. Llorca, Appl. Catal. B 127 (2012) 59–67.
[31] E. Suzuki, Y. Ono, Bull. Chem. Soc. Jpn. 61 (1988) 1008–1010.
[32] S. Kannan, C.S. Swamy, Appl. Catal. B 3 (1994) 109–116.
[33] J.N. Armor, T.A. Braymer, T.S. Farris, Y. Li, F.P. Petrocelli, E.L. Weist, S. Kannan, C.S. Swamy, Appl. Catal. B 7 (1996) 397–406.
[34] C. Gennequin, T. Barakat, H.L. Tidahy, R. Cousin, J.F. Lamonier, A. Aboukaïs, S. Siffert, Catal. Today 157 (2010) 191–197.
[35] Z. Jiang, J. Yu, J. Cheng, T. Xiao, M.O. Jones, Z. Hao, P.P. Edwards, Fuel Process. Technol. 91 (2010) 97–102.
[36] H. Wang, H. Ma, W. Zheng, D. An, C. Na, ACS Appl. Mater. Interfaces 6 (2014) 9426–9434.
[37] F. Li, Q. Tan, D.G. Evans, X. Duan, Catal. Lett. 99 (2005) 151–156.
[38] Y. Zhao, Q.Z. Jiao, C.H. Li, J. Liang, Carbon 45 (2007) 2159–2163.
[39] M.-Q. Zhao, Q. Zhang, W. Zhang, J.-Q. Huang, Y. Zhang, D.S. Su, F. Wei, J. Am. Chem. Soc. 132 (2010) 14739–14741.
[40] Y. Seida, Y. Nakano, Water Res. 36 (2002) 1306–1312.
[41] United States Environmental Protection Agency, Clean Water Act Priority Pollutant List, 1982, Code of Federal Regulations 40CFR 423 Appendix A.
[42] United States Environmental Protection Agency, Health and Environmental Effects Profile for Aminophenols, 1985.
[43] H.A. Thompson, G.A. Parks, G.E. Brown, Clays Clay Miner. 47 (1999) 425–438.
[44] K. Klemkaite, I. Prosycevas, R. Taraskevicius, A. Khinsky, A. Kareiva, Cent. Eur. J. Chem. 9 (2011) 275–282.
[45] D. Tichit, S. Ribet, B. Coq, Eur. J. Inorg. Chem. 2001 (2001) 539–546.
[46] D. Tichit, M.N. Bennani, F. Figueras, J.R. Ruiz, Langmuir 14 (1998) 2086–2091.
[47] J. Rocha, M. del Arco, V. Rives, M.A. Ulibarri, J. Mater. Chem. 9 (1999) 2499–2503.
[48] S. He, C. Li, H. Chen, D. Su, B. Zhang, X. Cao, B. Wang, M. Wei, D.G. Evans, X. Duan, Chem. Mater. 25 (2013) 1040–1046.
[49] G.-L. Tian, M.-Q. Zhao, B. Zhang, Q. Zhang, W. Zhang, J.-Q. Huang, T.-C. Chen, W.-Z. Qian, D.S. Su, F. Wei, J. Mater. Chem. A 2 (2014) 1686–1696.
[50] R.C. Peterson, G.A. Lager, R.L. Hitterman, Am. Mineral. 76 (1991) 1455–1458.
[51] R. Allmann, H.P. Jespen, Neues Jahrb. Mineral.-Abh. (1969) 544–551.
[52] A.L. Patterson, Phys. Rev. 56 (1939) 978–982.
[53] D.A. Young, Phase Diagrams of the Elements, University of California Press, Oakland, 1991.
[54] M. Varon, I. Ojea-Jimenez, J. Arbiol, L. Balcells, B. Martinez, V.F. Puntes, Nanoscale 5 (2013) 2429–2436.
[55] N. Cabrera, N.F. Mott, Rep. Prog. Phys. 12 (1948) 163–184.
[56] S. Wunder, Y. Lu, M. Albrecht, M. Ballauff, ACS Catal. 1 (2011) 908–916.
[57] H. Ma, H. Wang, C. Na, Appl. Catal. 163 (2015) 198–204.
[58] Z.D. Pozun, S.E. Rodenbusch, E. Keller, K. Tran, W. Tang, K.J. Stevenson, G. Henkelman, J. Phys. Chem. C 117 (2013) 7598–7604.
[59] J.-M. Song, S.-S. Zhang, S.-H. Yu, Small 10 (2014) 717–724.
[60] Z.-X. Zhang, X.-W. Wang, K.-L. Wu, Y.-X. Yue, M.-L. Zhao, J. Cheng, J. Ming, C.-J. Yu, X.-W. Wei, New J. Chem. 38 (2014) 6147–6151.
[61] X.-W. Wang, K.-L. Wu, K. Liu, W.-Z. Wang, Y.-X. Yue, M.-L. Zhao, J. Cheng, J. Ming, X.-W. Wei, X.-W. Liu, CrystEngComm 17 (2015) 734–739.
[62] M. Mandal, S. Kundu, S.K. Ghosh, T.K. Sau, S.M. Yusuf, T. Pal, J. Colloid Interface Sci. 265 (2003) 23–28.
[63] S.K. Ghosh, M. Mandal, S. Kundu, S. Nath, T. Pal, Appl. Catal. A 268 (2004) 61–66.
[64] C. Gómez-Lahoz, F. García-Herruzo, J.M. Rodríguez-Maroto, J.J. Rodríguez, Water Res. 27 (1993) 985–992.
[65] J.A. Ulman, W., Verstraeten, M.A., Cook, W., Verleye, L.J., Guilbault, Separating metals from waste water, in: U.S.P.a.T. Office, Morton International, Inc., Chicago, IL, 1994, 6.
[66] C.L. Alexander, A.M., Mariniello, B.A., McBride, M.M., Cook, D.A. Dunn, Waste treatment of metal plating solutions, in: U.S.P.a.T. Office, Morton International Inc., 2000.
[67] The Dow Chemical Company, VenMetTM Borohydride Solution, 2013.
[68] Kemira Oyj, Sodium borohydride products.
[69] T. Vincent, E. Guibal, Langmuir 19 (2003) 8475–8483.
[70] H. Ma, C. Na, ACS Catal. 5 (2015) 1726–1735.
[71] X. Liu, C. Prewitt, Phys. Chem. Miner. 17 (1990) 168–172.
[72] N. Spiridis, D. Wilgocka-Ślęzak, K. Freindl, B. Figarska, T. Giela, E. Młyńczak, B. Strzelczyk, M. Zając, J. Korecki, Phys. Rev. B 85 (2012) 075436.
[73] D.R. Lide, CRC Handbook of Chemistry and Physics, CRC Press, New York, 2006.
[74] P. Krishnan, S.G. Advani, A.K. Prasad, Int. J. Hydrogen Energy 33 (2008) 7095–7102.
[75] U.B. Demirci, P. Miele, Phys. Chem. Chem. Phys. 12 (2010) 14651–14665.
[76] V. Iablokov, S.K. Beaumont, S. Alayoglu, V.V. Pushkarev, C. Specht, J. Gao, A.P. Alivisatos, N. Kruse, G.A. Somorjai, Nano Lett. 12 (2012) 3091–3096.
[77] Y.-P. Sun, H.W. Rollins, R. Guduru, Chem. Mater. 11 (1998) 7–9.
[78] H. Hirai, N. Yakura, Polym. Adv. Technol. 12 (2001) 724–733.
[79] J.A. Lopez-Sanchez, N. Dimitratos, C. Hammond, G.L. Brett, L. Kesavan, S. White, P. Miedziak, R. Tiruvalam, R.L. Jenkins, A.F. Carley, D. Knight, C.J. Kiely, G.J. Hutchings, Nature Chem. 3 (2011) 551–556.
[80] P. Beaudot, M.E. De Roy, J.P. Besse, J. Solid State Chem. 161 (2001) 332–340.
[81] P. Beaudot, M.E. De Roy, J.P. Besse, J. Solid State Chem. 177 (2004) 2691–2698.